10th World Seminar on Seismic Isolation, Energy Dissipation and Active Vibration Control of Structures, Istanbul, Turkey, May 28-31, 2007

RESEARCH ACTIVITIES IN CHILE AND ARGENTINA ON BASE ISOLATION, PASSIVE ENERGY DISSIPATION AND VIBRATION CONTROL

Mauricio Sarrazin, María Ofelia Moroni, Rubén Boroschek, Ricardo Herrera
Dept. of Civil Engineering, University of Chile, Casilla 228/3 Santiago, Chile
sarrazin@ing.uchile.cl, mmoroni@ing.uchile.cl, rborosch@ing.uchile.cl, riherrer@ing.uchile.cl
Paul Roschke
Dept. of Civil Engineering, University of Texas A&M,Texas, USA
roschke@civil.tamu.edu
Miguel Tornello
National Technical University, Mendoza, Argentina
mtornell@frm.utn.edu.ar

ABSTRACT

The latest research activities in progress at the University of Chile and the National Technical University at Mendoza, Argentina on base isolation, passive energy dissipation, and vibration control are presented. These include analysis of seismic records obtained at seismic isolated structures, and shaking table test results from two scaled-model structures: a shear wall building with base isolation and a steel frame building with bracing made of a copper-based alloy. The scale models were subjected to different seismic inputs, including horizontal as well as vertical components. Analytical models were developed to reproduce the experimental results. The paper also includes the design and test of an energy dissipating device consisting of a Tuned Mass Damper (TMD) with magneto-rheological (MR) characteristics, and its application to a pedestrian bridge over a railroad right-of-way that exhibits accelerations of such a degree that people who use it are uncomfortable. Finally, the design, construction, instrumentation and analysis of recorded earthquake motions of a three story building with spring base isolation located at Mendoza, Argentina, are presented.

1. INTRODUCTION

A significant amount of research on base isolation, passive energy dissipation, and vibration control has been conducted in Chile and Argentina over the last years. Three base isolated buildings have been built in Chile and one is under construction. Two of them are hospitals, one is for educational purposes and the oldest one is for residential use. The latter has been instrumented since 1992 with a local array of accelerometers that have recorded approximately 40 small and moderate earthquakes. From these records, a clear reduction in the horizontal accelerations has been observed with some amplification in the vertical acceleration. In order to investigate the effect of more severe earthquakes, a scale-model of the instrumented building has been tested on a shaking table. The same facility has been used to study the effect of adding SMA copper-based bracing to a bare steel frame building.

A tuned mass vibration absorber with a controlable magneto-rheological semi-active damper has been studied for vibration control of a very flexible pedestrian overpass that serves a community near a railroad right-of-way.

In Mendoza, Argentina, a university residential building has been built on spring bearings for isolation from near-fault earthquakes. Large viscous damping was also added with the aim of controlling the base displacements.

Finally, with respect to bridges, many of them have been built recently with neoprene or natural rubber pads between piers and the superstructure. Three of them have been instrumented with local accelerometer networks. Although only moderate earthquakes have excited these structures in the last two years, seismic records obtained have permitted calibration of theoretical models and advancement in the knowledge of their seismic behavior.

Salient details of these research projects are presented in this paper.

2. SHAKING TABLE TESTS

2.1 Comunidad Andalucía Building (Brull, 2005, Munoz, 2005)

2.1.1 Model description

A 1:10 scale acrylic model of the Comunidad Andalucía building was constructed and tested on a small shaking table. Two support types were studied: high damping rubber bearings (HDRB) and sliding bearings. The same model was also tested for a fixed foundation. Dimensions of the model were 1 m x 0.6 m in plan and 1 m high. The elastic modulus of acrylic was 3353.8 MPa and the specific weight, 1.17 ton/m^3; both values were obtained experimentally. The wall thickness was 0.5 cm and the slab thickness, 1 cm. Figure 1 shows the model on the shaking table.

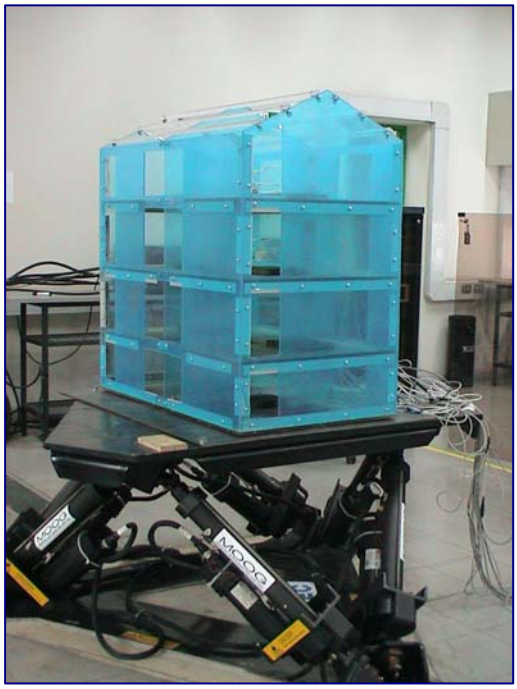

Figure 1 General view of the acrylic building model

Horizontal and vertical input accelerations were recorded, as well as horizontal and vertical accelerations at the first and fourth floors, and longitudinal displacements at the first and fourth floors.

Initially, pull-back tests were performed and fundamental periods and equivalent damping were obtained from the acceleration signals using both the method proposed by Ibrahim et al (1977) and the logarithmic decrement method. Fundamental periods of 0.086 and 0.069 sec in the longitudinal and transverse direction were obtained for the fixed base conditions with equivalent damping ratios of 3.8 and 3.9%, respectively. The model weighted 50.5 kgf and an additional 65.7 kgf was distributed in the four slabs.

Records from the March 3, 1985, Llolleo-Chile earthquake scaled both in time (scale factor = 2,236) and magnitude (scale factor = 2) were used. Unfortunately, due to limitations of the shaking table, the input acceleration to the scaled model differed sustantially from their real counterparts. This can be seen in Figure 2 where the response spectra for the original Llolleo N10E, the scaled record and the effectively registered record on the shaking table for a 5% damping are shown. This problem arose from the necessity of scaling the records in time thus shifting the frequency content to a high frequency region where the shaking table had a limited response.

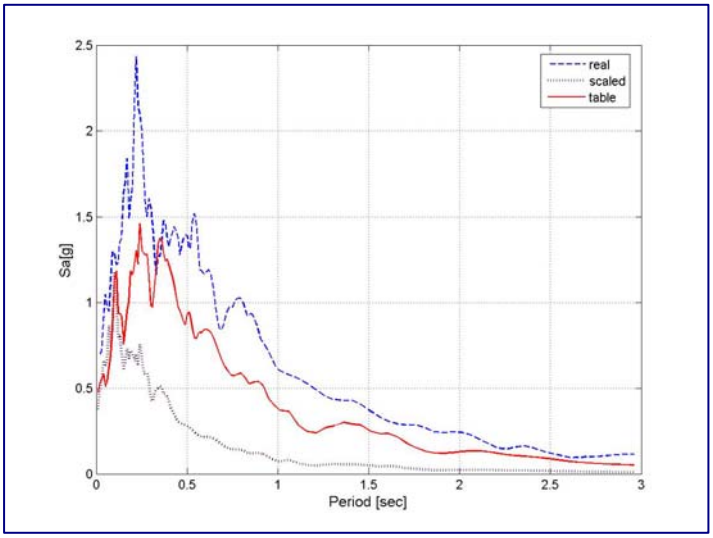

Figure 2 Response Spectra for Llolleo N10E

2.1.2 HDRB

In this case four bearings were located at the middle of each side of the base of the building model. A rubber shear modulus of 0.85 MPa and equivalent damping of 7.6% were obtained for samples of 3 x 3 x 0.28 cm strained at 50%. Based on these values, the following dimension were obtained: 10 cm total rubber thickness, 3.9 cm diameter, and 12.84 cm total height (Brull, 2005).

Three pull-back tests were performed with different added weights; fundamental periods and equivalent damping are shown in Table 1. It was found that values of the period and damping are quite similar for both directions, thereby corroborating the SDOF behavior of these structures. The period and damping increased with increasing weight. Because of the slenderness of the rubber bearings an important bending effect on its lateral stiffness was found, with a value of one half of the shear only stiffness.

Table 1 Period and equivalent damping for scale model building with HDRB

Added weight (kgf)	Period (sec)		Equivalent damping (%)	
	Longitudinal	Transverse	Longitudinal	Transverse
40	0.449	0.447	7.54	7.92
64	0.503	0.491	8.30	8.87
100	0.573	0.551	9.8	9.48

The model with an added weight of 100 kgf was tested on the shaking table. Five records were applied in the longitudinal direction and two in both horizontal directions. As previously mentioned, due to limitations of the shaking table, the effect of the isolation was rather low, although some reduction in peak accelerations was noticed. Shear deformation at the bearings reached 28.5%. A predominant frequency of 1.7 Hz was determined from the records at the 4th floor, using Fourier analysis.

2.1.3 Sliding bearings

Eight friction bearings and two rubber bearings were used to provide restoring forces (Figure 3). The friction bearings consisted of a Teflon sheet, 4.5 cm in diameter and 0.5 cm thick that could slide on a square polished stainless steel plate that had dimensions of 10 by 10 cm and 2 mm thick. The friction coefficient varied between 0.11 to 0.16 for lubricated and non lubricated conditions, respectively. The rubber bearings were 3.9 cm in diameter and 12.6 cm tall; at both extremes 0.5 cm thickness square plates were added to join the bearings through bolted connections to the shaking table and to the base of the structure (Muñoz, 2005).

During the test, an additional weight of 48.75 kgf was applied to each floor in order to obtain a fundamental period of 1.12 sec, which would represent a 2.5 sec period in the prototype building. Although similar records to those applied to the previous model were selected, peak accelerations at the shaking table were much larger than before. Figure 4 shows the peak

Figure 3 Friction and rubber bearings

acceleration recorded at the fourth floor in the isolated and conventional buildings as a function of the input peak acceleration measured at the shaking table. Peak accelerations in the model with sliding bearings were about 20% less than the input peak acceleration, and peak accelerations in the conventional model were 40 to 90% larger than the peak acceleration in the sliding model. Figure 5 shows the Arias intensity calculated at the fourth floor in the model with sliding bearings and in the fixed base model, as a function of the Arias intensity of the input acceleration; this function represents the energy that is transferred to the structure. In most cases, the energy transferred to the isolated model is less than that transferred to the conventional model.

Maximum shear deformations in the rubber bearings varied between 1.2 and 1.9 cm and the permanent deformation varied between 0.01 and 0.4 cm for the different records, thus indicating that the rubber bearing restoring forces were effective in controlling the final displacements of the base.

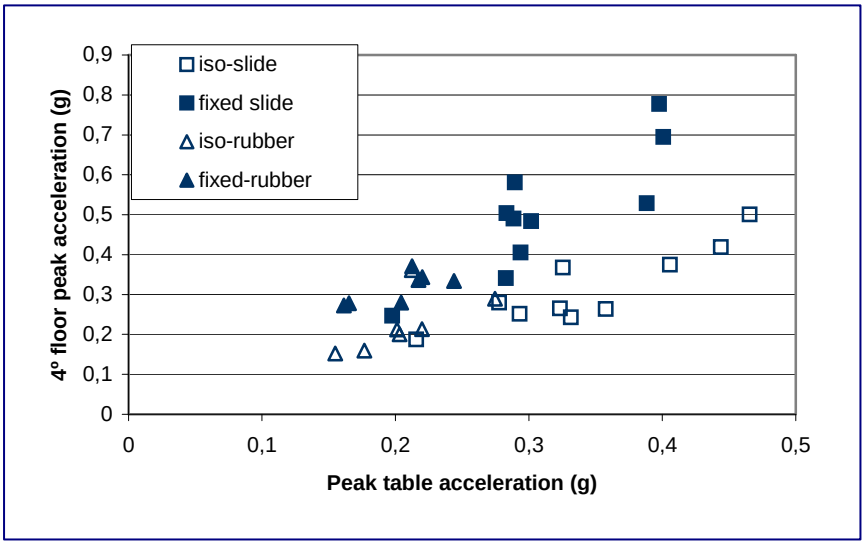

Figure 4 Peak acceleration comparison

2.2 Effect of SMA Braces in a Steel Frame Building (Valdivieso, 2006).

Shape Memory Alloys (SMA) are metallic alloys that can undergo large strains and recover their initial configuration after unloading or by heating, without any permanent deformation. They dissipate energy in the loading-unloading process. This behavior makes them suitable to be used as seismic dissipation devices. Damping devices based on SMA CuAlBe wire were installed in the longitudinal direction of a scaled model of a three-story steel moment resistant frame building.

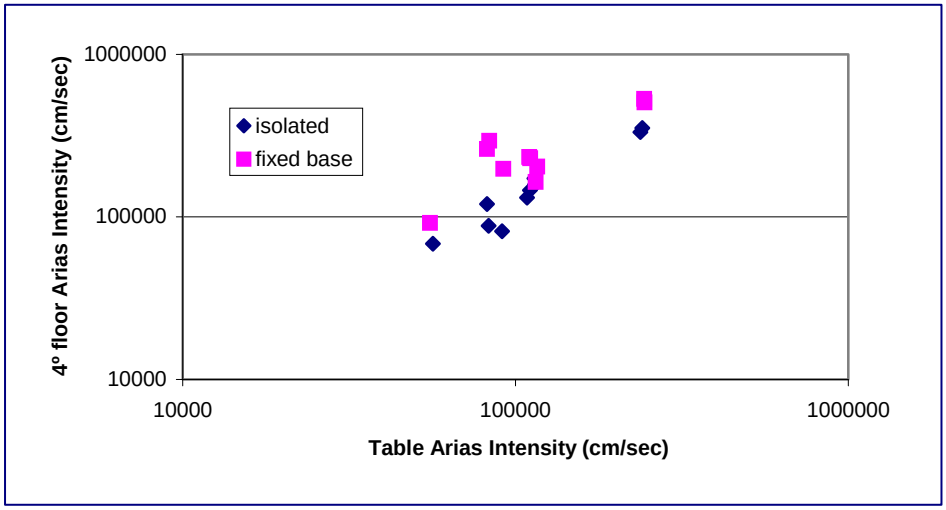

Figure 5 Arias Intensity comparison

Shaking table tests were performed on the bare frame structure and on a braced one. The results of this research are presented in detail in another paper in this conference and therefore are not described here. The model used can be seen in figure 6.

Figure 6 Steel frame scaled model

3. CONTROL OF PEDESTRIAN BRIDGE VIBRATION USING AN MR-TUNED MASS DAMPER AND A GA-FUZZY CONTROLLER

3.1. Introduction

Pedestrian bridges serve a vital function of providing ease of travel for human traffic (figure 7). Due to relatively small live load requirements they can be constructed to span long distances with a modest amount of mass and stiffness. Unfortunately, this combination of geometry and light-weight materials can lead to structures that are susceptible to lateral, vertical or combined modes of vibrations that result from pedestrian and environmental loads. Engineering attempts to

minimise these undesirable vibrations and improve serviceability are often subdivided into three categories: passive, active, and semi-active control. Since active control is usually considered to be impractical due to high initial and maintenance costs, only passive and semi-active control approaches are discussed in what follows.

Figure 7. San Bernardo Overpass

A pedestrian bridge over a railroad right-of-way in Santiago, Chile, has been observed to accelerate to such a degree that people who use it are uncomfortable. The approach toward vibration reduction that is described bellow relies on a combination of two tuned-mass dampers (TMD) and an optimal fuzzy controller. Displacement and acceleration amplification functions for a two degree-of-freedom linear model of the bridge and TMD are developed in conjunction with a finite element analysis of the entire structure. The two prototype devices consist of a spring mass, a flexible lamina, and a controllable magneto-rheological (MR) damper.

After verification of its accuracy, a simplified model of the bridge was used for a series of numerical simulations aimed at developing a robust controller. A fuzzy model of the behaviour of a small MR damper was developed from experimental data using a neuro-fuzzy approach. The damper was installed in a prototype TMD device that was placed on a pedestrian bridge. Experimental tests of the effectiveness of the TMD were conducted using prompted individual and group walking. A second prototype device that has a low profile is considered for installing in a pedestrian bridge. Moreover, a second prototype TMD that has a low profile is being constructed. Numerical simulations of the behaviour of this device are being undertaken in order to develop a set of optimal controllers that are optimised for the San Bernardo structure. These fuzzy controllers that operate a semi-active MR damper are determined using an NSGA II genetic algorithm that treats multiple objectives during the same simulation. A bridge designer or retrofit engineer is given the opportunity to select a fuzzy controller from a set of controllers based either on peak displacement, root-mean-square displacement, peak acceleration, or root-mean square acceleration, or combinations of these objectives. Results from experimental testing and numerical simulations of these two prototype devices show that passive and semi-active control can effectively reduce undesirable vibrations from human traffic on a pedestrian bridge.

3.2. Equivalent Modal Mass of Bridge

The pedestrian bridge selected for this study is the San Bernardo overpass which crosses over a railroad and is located in a suburb of Santiago, Chile (Figure 7). While the structure is still in service, it has been reported that pedestrians have uncomfortable accelerations while traversing the structure. Basic properties of this bridge are outlined in Table 2. Although the bridge is continuous with multiple supports and has a variable cross-section between supports, the central span provides the dominant contribution to the first mode of vibration. Use of a finite element code and the analysis that is outlined below are used to find an equivalent modal mass for a single degree of freedom structure.

If damping is neglected for simplicity, a single degree of freedom has the following well-known equation of motion:

$$M\ddot{y} + Ky = F(t) \tag{1}$$

where M is the mass matrix, K is the stiffness matrix, y is the displacement, and $F(t)$ is a forcing function. For a multiple degree of freedom structure the modal equations for the n^{th} mode are as follows (Biggs, 1964):

$$\ddot{A}_n \sum_r M_r \phi_{rn}^2 + A_n \sum_g K_g \phi_{\Delta gn}^2 = \sum_r F_r \phi_{rn} \tag{2}$$

where ϕ_{rn} is the modal shape of the n^{th} mode, M_r is the mass associated with the r^{th} degree of freedom, K_g is the stiffness of the spring g, $\phi_{\Delta gn}$ is the relative modal shape between the degrees of freedom connected by the spring g, A_n is the modal degree of freedom, and F_r is the force applied to the r^{th} degree of freedom.

If it is assumed that the applied load is a single load applied at the k^{th} degree of freedom and that the mode shapes are normalised with respect to the mass then it follows that:

$$\sum_r M_r \phi_{rn}^2 = 1 \tag{3}$$

and Equation (2) becomes

$$\ddot{A}_n + A_n \sum_g K_g \phi_{\Delta gn}^2 = F_k(t) \phi_{kn} \tag{4}$$

The displacement at the point of application of the load is:

$$y_{kn}(t) = A_n \phi_{kn} \tag{5}$$

Multiplying through each term of equation (3) by ϕ_{kn} leads to the following expression:

$$\ddot{y}_{kn} + y_{kn} \sum_g K_g \phi_{\Delta gn}^2 = F_k(t) \phi_{kn}^2 \tag{6}$$

By analogy with equation (1):

$$M = \frac{1}{\phi_{kn}^2} \tag{7}$$

From results of supporting finite element analyses, use of Equation (7), and vibration experiments on the structure, the equivalent mass and stiffness of a single degree of freedom (SDOF) representation of the bridge are listed in Table 2.

Table 2. Fundamental Properties of San Bernardo Bridge and TMD

Property	Value
Equivalent Mass (kg)	19,439
Equivalent SDOF stiffness (Tonf/cm)	3.702
Percent of Critical Damping	2.8
Fundamental Period of Bridge (sec)	0.46
Mass of TMD Prototype 1 (kg)	142.7
Mass of TMD Prototype 2 (kg)	186

3.3. Experimental Tests with Prototype TMD 1

In order to accurately simulate the behaviour of an RD-1005 MR damper, a series of performance tests was conducted with the aid of a steel frame and a shake table. One end of the damper was attached to a rigid frame that is attached to the floor and the other end was displaced by a commanded motion of the shake table. Data from these experiments were used to adjust parameters of a fuzzy model of the damper so that correct force of the damper is predicted for given values of displacement, velocity, and applied voltage from a voltage controlled current source (VCCS). Details of this procedure that leads to a Takagi-Sugeno-Kang fuzzy representation are available elsewhere (Oh *et al.* 2004; Kim and Roschke 2006; Roschke and Likhitruangslip 2003). Figure 8 shows a fuzzy surface of the force resisted by the MR damper for

a range of velocity and voltage values. Two, four, and three membership functions are used for the displacement, velocity, and voltage input functions, respectively.

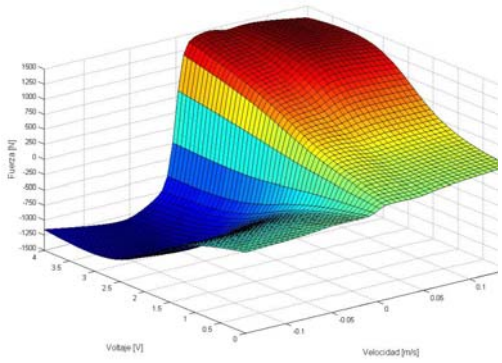

Figure 8. Fuzzy Surface of MR Damper Force

After an accurate numerical model of the MR damper was available, numerical simulations led to design and fabrication of prototype TMD 1 as shown in Figure 9. A variable number of springs are attached between a rigid frame and a rigid sprung mass that moves vertically. The RD-1005 MR damper is also attached between the frame and a steel bar that is attached to the lower movable mass. A set of holes in an adjustable mechanical arm allows for a variable position of the damper, thereby amplifying or decreasing the displacement of the piston for a given displacement of the tuned mass.

Figure 9. Prototype TMD 1

Figure 10. Pedestrian Loading

Prototype TMD 1 was placed on the walking surface of the San Bernardo bridge for testing with pedestrian loadings. Acceleration of the structure was measured at the center location on the bridge using accelerometers. Two sets of tests were conducted on the bridge. In the first set of tests a single pedestrian traversed the bridge at a steady pace. In the second set of tests six pedestrians walked across the main span of the bridge in a cadenced walk (see Figure 10). For this experimental study the MR damper was operated only in a passive mode.

3.4. Experimental Results

Tests were conducted consisting of a group of six adults that walked across the bridge in synchronous motion. The baseline case is the response of the bridge without the TMD on the walking surface. Configuration 1 has the TMD in place but without an MR damper and without guide plates. Configuration 2 is similar but has 4 guide plates. Configuration 3 has the MR damper in position 2 with 0 V and 4 guide plates. Configuration 4 has the MR damper in position 3 with 0 V and 4 guide plates. Table 3 lists the percentage reduction of RMS and peak accelerations in comparison with the uncontrolled case.

Especially notable is the reduction of more than 60% in both RMS and peak acceleration for Configuration 3.

Table 2. Reduction in Acceleration for Test Series 2

Load	Acceleration	Configuration 1 (%)	Configuration 2 (%)	Configuration 3 (%)	Configuration 4 (%)
6 Pedestians	**RMS**	45.2	26.8	63.7	33.3
	Peak	44.7	31.4	63.5	29.4

3.5. Numerical Simulation with Prototype TMD 2

The first prototype damper was placed on the walking surface of the pedestrian bridge in order to determine effectiveness of the device in damping pedestrian vibration. However, for the TMD to be installed beneath the main girder of the bridge and to maximize clearance of railway traffic below the structure, a low-profile version of the TMD has been designed and is being manufactured. This section of the paper is dedicated to describe prototype TMD 2 damper and report results of numerical simulation with this device installed under the San Bernardo bridge. Finally, a number of different kinds of controllers are investigated for comparative purposes.

3.5.1. Description of Prototype TMD 2

As shown in Figure 11, for prototype TMD 2 two rotating masses are attached to the girder of the bridge by means of two pins and steel rods. The distance from each pin to the mass, $\boldsymbol{m_d}$ is denoted by $\boldsymbol{L_1}$. A flexible elastomer serves as an interface between the two rotating rods that support the masses and, along with a shear key, restrict the motion of the two masses to be symmetric about the pins. A set of adjustable springs are attached to the underside of the bridge girder and the rotating rods at a distance $\boldsymbol{L_1 + L_2}$ from each pin. An RD-1005 MR damper is placed between the vertical steel members at a distance $\boldsymbol{L_3}$ from the rotating pins (Figure 11) and provides a variable resisting force $\boldsymbol{F_d}$ to the rotational motion of the two arms.

After writing expressions for kinetic energy, potential energy, and external work for the prototype TMD 2 system and using assumptions related to small deflection approximations, application of Lagrange's equations of motion leads to the following system of simultaneous equations:

$$\begin{bmatrix} m_s + 2m_d & 2m_d \\ 2m_d & 2(m_d + \dfrac{I_0}{L_1^2}) \end{bmatrix} \begin{Bmatrix} \ddot{u}_s \\ \ddot{u}_d \end{Bmatrix} + \begin{bmatrix} k_s & 0 \\ 0 & 2k_d \dfrac{L_1 + L_2}{L_1} \end{bmatrix} = \begin{Bmatrix} P \\ 2F_d \dfrac{L_3}{L_1} \end{Bmatrix} \tag{8}$$

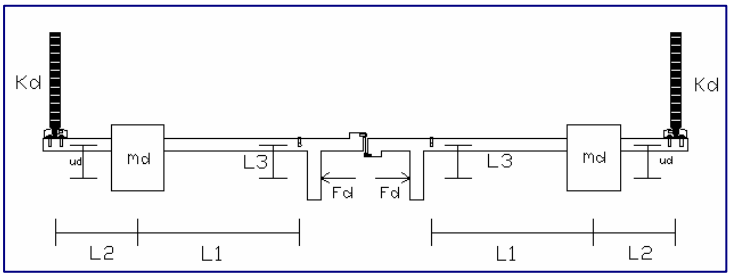

Figure 11. Prototype TMD 2

where u_s is the absolute displacement of the equivalent mass of the bridge deck; u_d is the relative vertical displacement of the rotating TMD mass, m_s and m_d are the mass of the bridge and rotating mass, respectively; k_s and k_d are stiffness of the SDOF representation of the bridge deck and the TMD springs, respectively; I_0 is the rotational moment of inertia of each rotating mass about its own centroidal axis; F_d is the resisting force of the MR damper, and *P* is the excitation load acting on the bridge deck due to pedestrians traversing the structure. This two degree of freedom system of equations is solved through time by means of Matlab and Simulink code (The Mathworks 2006). Similar to the case for prototype TMD 1, the resisting force

provided by the MR damper is predicted by the fuzzy inference system (FIS) described earlier when the displacement, velocity, and voltage are known.

3.6. Pedestrian Loads

Several types of pedestrian loads were considered for numerical simulation with prototype TMD 2. While the experimental work discussed previously for prototype TMD 1 used human subjects to generate live experimental loads, for the numerical simulation that follows it was necessary to employ artificially generated loads. To this end, a simple sinusoidal signal with an amplitude of 1,000 N and various frequencies was used to generate the first set of pedestrian loads. The second set of loads were generated from a numerical model proposed by Ungar *et al.* (2004). Dwell times of the footfall model were adjusted to be slightly shorter so
that one of the primary excitation frequencies approximately matches the fundamental 2.0 Hz observed on the San Bernardo bridge.

3.7. GA-Fuzzy Controller

For control of the MR damper, a fuzzy inference system (FIS) was selected due to its relative simplicity and ability to handle nonlinear problems. Although the bridge structure is assumed to behave in a linear fashion, addition of the low profile device with an embedded MR damper creates a nonlinear system. As described in other publications (e.g. Kim and Roschke 2006) a tenable approach for satisfactory control of these systems is to construct a prototype Mamdani fuzzy logic controller and then use a genetic algorithm to optimize parameters of the membership functions in the rule base. Inputs for the FIS were taken to be the absolute acceleration of the bridge girder at midspan and a delayed signal from the same transducer. That is, two accelerations from the same accelerometer were used as input to the controller in order to increase reliability of the system. Output from the FIS is simply a command voltage to a voltage control current source (VCCS) that sends current to the MR damper. Here, optimization was performed with an NSGA II genetic algorithm that has been adopted to solve problems related to control of civil engineering structures (Deb *et al.* 2002).

Although the NSGA II algorithm has successfully solved problems with four objectives, here the primary concern was to reduce accelerations as much as possible so that people using the bridge were comfortable during their time on the structure. Therefore, objectives for minimization that were considered simultaneously were the peak and root mean square (RMS) accelerations at the center of the main span. A total of 100 generations were computed along with a population of 100 chromosomes; this corresponded to 10,000 evaluations of the response time history. Each chromosome contained real-valued information concerning the parameters of the membership functions that were varied by the GA.

A number of different controllers were considered in this study for comparative purposes. The performance of each controller was normalized by the uncontrolled response of the structure. The first pair of controllers were passive. That is, the resistance of the MR damper was set to be either minimum (i.e. zero Amperes are applied to the damper coil) or maximum (the saturation level of Amperes is applied). A relatively simple classical groundhook controller was also used to facilitate an objective comparison with the NSGA II fuzzy controller. Finally, an NSGA II fuzzy logic controller (GA-FLC) was selected from a final, optimized, population of 100 controllers for its ability to reduce peak acceleration.

Table 4. Controller Effectiveness for Pedestrian Load

Controler	Normalized Peak Acceleration	Normalized RMS Acceleration	Peak MR Force (N)
Passive off	0.782	0.794	339
Passive On	0.785	0.777	603
Groundhook	0.555	0.628	1070
GA-FLC	0.503	0.556	912

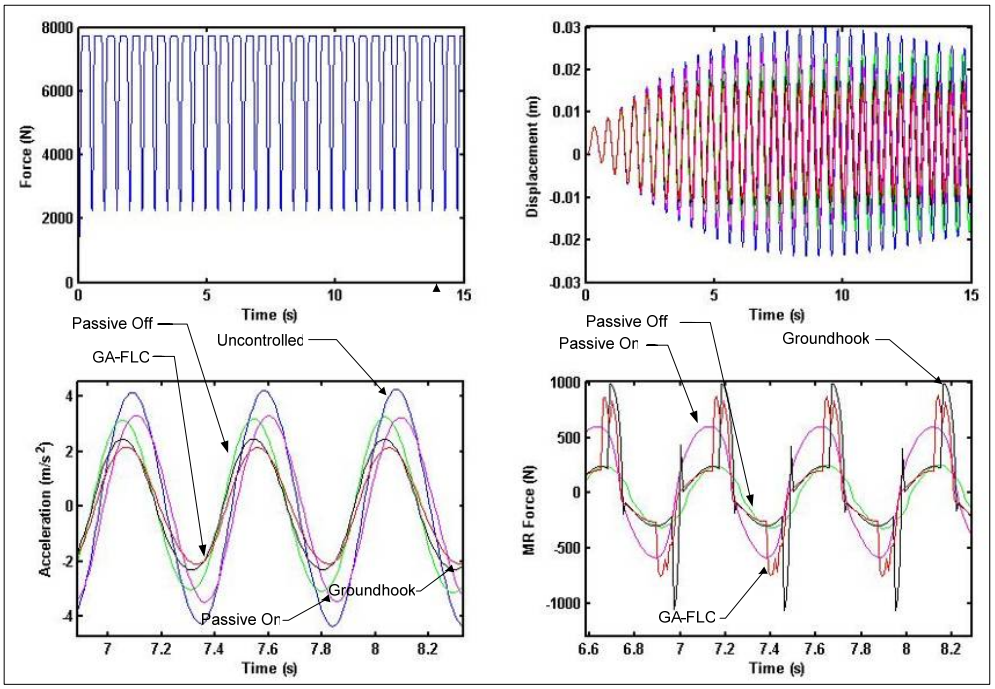

Figure 12. Fast Pedestrian Load, and Uncontroled and Controled Displacement, Acceleration, and MR Damper Force for Fast Pedestrian Load.

Due to space limitations results for controlled responses of the bridge are reported in Table 4 only for a concatenated combination of slow, medium, and fast pedestrian loads generated with a modified form of the Ungar *et al.* model (2004). Results indicate that both the groundhook and GA-FLC controllers are able to substantially reduce accelerations in comparison with the passive controllers that specify a constant current to the MR damper for the duration of the loading. As a second brief example, Figure 12 shows a time history of the force imposed by a 'fast' footfall and the displacement, acceleration, and MR force elicited by the load for each controller. Significant reductions in displacement and acceleration are evident for both semi-active controllers in comparison with the uncontrolled bridge response.

4. SPRING ISOLATED BUILDING IN MENDOZA, ARGENTINA

4.1. Introduction

A building belonging to the Technical National University (TNU) in Mendoza, Argentina was isolated by means of spring isolators and viscous dampers. The spring bearings, instead of the more traditional rubber ones, were selected for several reasons: a) economical (they were cheaper than the rubber isolators because the maker was willing to make a considerable discount for introducing the product), b) because of the near fault location of the building it was necessary to provide a large amount of damping in order to control displacements, and finally c) the instalation was intended to test a less conventional type of base isolation device. The spring and damping devices shown in Figure 13 were provided by GERB, Germany.

a) Spring support b) Damping device

Figure 13 GERB's spring support and viscous damper.

4.2. Characteristics of the base isolated structure

The base isolated structure is one of three student housing buildings at TNU, Mendoza campus. The buildings are three-storied reinforced concrete and masonry construction. One of the building is base-isolated and the other two have traditional fixed foundations. A general picture of the isolated building can be seen in Figure 14. The building is 7.60 m by 8.10 m in plan and has a natural period of vibration of 0.15 s for fixed base. Its total weight is 2600 KN.

Figure 14. Isolated residential building

The isolation system consists of four spring isolators and four visco-elastic dampers. These springs are grouped into a pack whose design is a function of vertical and horizontal stiffness and the static and dynamic demand produced by earthquakes. Table 5 contains the characteristics of the isolation system. The spring isolators were designed for a horizontal frequency of 1.00 to 1.5 Hz and vertical frequency of 3.00 to 3.50 Hertz.

Figure 15 Viscous damper and springs bearing at the building's basement.

Table 5: Dynamic Characteristic of the Isolation System (SP and EVD)

Parameter	Value
Vertical load nominal capacity	768 KN
Vertical stiffness	29500 KN/m
Horizontal Stiffness	3940 KN/m
Horizontal damping	26%
Vertical damping	13%

4.3. Evaluation for near-fault earthquakes.

The response of the isolated building as well as the fixed-base twin building were evaluated analytically using the SAP2000 program for a set of historical near-fault records (Table 6).

Table 6. Near-fault motions (Collapse Accelerograms (WDA) data base).

Event	Date	Station	Comp.	Mag	Epic. Distance (km)	Ground	P_D (cm-s)	PGA (g)	PGV (cm/s)	PGD (cm)
Tabas Iran	16/09/78	Tabas 9101	TR	7.4	3.00	Soft	13.2	0.85	121.4	94.60
Imperial Valley	15/10/79	Bond Corner	230º	6.9	2.50	Soft	24.9	0.78	45.90	14.90
Coalinga	22/07/83	Transmitter Hill	360º	5.7	9.20	Rock	4.70	1.08	39.70	5.40
Loma Prieta	17/10/89	Corralitos Eureka	N-S	7.1	5.10	Firm	8.40	0.64	55.20	10.90
Loma Prieta	17/10/89	Los Gatos	Fault Normal	7.1	3.50	Firm		0.72	173	64.70
Cape Mendocino	25/04/92	Cape Mendocino	N-S	7.0	8.50	Rock	4.90	1.50	127.40	41
Northridge	17/01/94	Tarzana Cedar Hill Nursery	E-W	6.7	17.5	Firm	32.4	1.78	113.60	33.20
Northridge	17/01/94	Rinaldi Receiving Station	228º	6.7	7.10	Soft	11.1	0.84	170.30	33.40
Kobe	17/01/95	Kobe Observat. JMA	N-S	6.9	0.60	Firm	20	0.82	81.30	17.70
Chi-Chi Taiwan	29/09/99	TCU084	E-W	6.9	10.40	Firm	11.6	1.16	114.7	31.40
Duzce Turkey	12/11/99	Lamont375	N-S	7.3	8.20	Firm	7.90	0.97	36.50	5.50

Where:

Ground	USGS Clasification	Wave Velocity Shear
Rock	A	> 750 m/s
Firm	B	360 a 750 m/s
Soft	C y D	< 360 m/s

and P_D = Destructive Potencial (Araya and Saragoni, 1984)

Two different isolation system were evaluated: a) an elastomeric isolating system with lead core (equivalent damping 15%) and b) a spring isolation system with viscous dampers that provide 26% damping for longitudinal input and 13% for vertical input. The average displacement response of the spring system was only 34% of the response of the elastomeric system, while the reduction of accelerations was larger for the later.

The forces developed on a first story column were also studied. For the spring system, average maximum shear forces and maximum normal forces showed a reduction of 46% with respect to the fixed- base building. The maximum bending moment was reduced to 42% and 49% of the fixed-base building case, for the elastomeric and spring systems, respectively.

4.4. Instrumentation

Both the isolated building and the fixed-base building were instrumented with a total of 12 acceleration sensors. The location of these sensors is described in Table 7.

Table 7. Characteristic and location of instruments

Chanel	Direction	Location	Characteristic	Model
1	E - O	Under isolated building	Triaxial (2g)	Altus K2
2	S - N			
3	Vertical			
4	S – N	At the center of gravity on roof of fixed-base building	Triaxial (2g)	Kinemetrics (FBA EST)
5	E – O			
6	Vertical			
7	E – O	N-E corner of bottom slab of isolated building.	Uniaxial (2g)	Kinemetrics (ESU)
8	S – N	Roof of isolated building	Uniaxial (2g)	Kinemetrics (ESU)
9	E – O	Roof of isolated building	Uniaxial (2g)	Kinemetrics (ESU)
10	E – O	At center of gravity of bottom slab in the isolated building	Triaxial (2g)	Kinemetrics (FBA EST)
11	S – N			
12	Vertical			
	E – O S – N Vertical	Structures Laboratory (Ceredetec – Department of Civil Engineering)	Triaxial (1g)	Kinemetrics SSA2

4.5. Results from actual records

Seventeen records of low intensity earthquakes have been obtained since the network of instruments was installed. From these records only three have a PGA greater than 0.01 g and one has a PGA larger than 0.1g. Table 8 contains a summary of results for the largest record, registered on August 5, 2006.

Table 8. Comparison of peak accelerations for isolated and non-isolated building, 05-08-2006 earthquake.

AT ISOLATION SYSTEM (G)			ABOVE ISOLATION SYSTEM (G)			AT ROOF OF ISOLATED BUILDING (G)			AT ROOF OF FIXED BASE BUILDING (G)		
E-W	VERT	N-S	E-W	VERT	N-S	E-W	VERT	N-S	E-W	VERT	N-S
12.5	5.3	9.8	8.0	6.8	8.3	9.1	-	7.6	24.6	12.4	40.6

The comparison of peak accelerations for the earthquake of August 5, 2006 shows a very favorable result for the isolation system in reducing the peak accelerations in the building.

5. ANALYSIS OF SEISMIC RESPONSE OF MARGA MARGA BRIDGE FOR 2007-06-20 EARTHQUAKE. ANALITICAL RESULTS CONSIDERING DIFFERENTIAL SUPPORT MOTIONS.

5.1. Introduction

The Marga-Marga bridge is located in Vina del Mar, Chile. It is the first bridge in the country with a superstructure supported on HDRB. The characteristics of this bridge were described before in a previous version of this seminar (Sarrazin et al., 2001). A general view can be seen in figure 16.

An analysis of records obtained from a magnitude 4.4 earthquake that shook the Vina del Mar area on the 20th of June, 2006, is presented below. A finite element model was developed

with the SAP2000 program, as shown in Figure 17, and analytical results were compared with actual ones. Two different cases were considered: first, sincronic earthquake motion for all supports, equal to the record registered on rock; and, second, different earthquake motions at each pier and abutments using the records registered at different points (bottom of pier C4, free field in the valley, free field on rock, and abutments).

Figure 16. General view of Marga Marga bridge

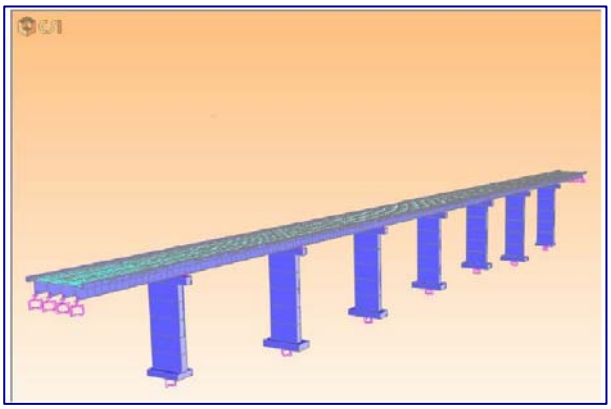

Figure 17. Finite element model

5.2 Records from June 20, 2006, earthquake.

The bridge is instrumented with a network of 24 accelerometers that have recorded several small to medium size earthquakes. Figure 18 shows the location and direction of sensors on the bridge. In addition, there is a triaxial accelerometer installed on rock near the south abutment and another triaxial sensor at a free surface 30 m downstream from pier 4. A profile through the valley is shown in Figure 19. An important effect of soil amplification should be expected from such a soil profile. Figures 20 and 21 show the acceleration records for the longitudinal and transverse directions, respectively. In them, a clear effect of amplification can be appreciated if the records on rock and at the free surface of valley are compared.

5.3. Analysis of results.

Figure 22 shows the longitudinal acceleration for the records at the free surface and the rock outcroping near the south abutment. A considerable effect of local soil amplification can be seen in this figure. The differences are apparent.

Figures 23 and 24 show the longitudinal and transversal acceleration components at the bottom of pier C4 and at free field on the valley surface. An important soil-structure interaction can be concouded from these figures, considering that without the influence of the structure this two records should be very similar in both directions.

Finally, Table 9 shows a **c**omparison of error with respect to registered records from two analytical models: a) considering differential motions between supports and b) with uniform earthquake input. In the case of the first of these models, the following motions were considered at the different supports: at both abutments, record registered on rock, near south abutment; for the piers, record registered at bottom of pier C4, with the exception of piers C1, C6 and C7 where the free surface record was used. The total error is reduced from 30% for the model with uniform input to 19% for model with differential motion.

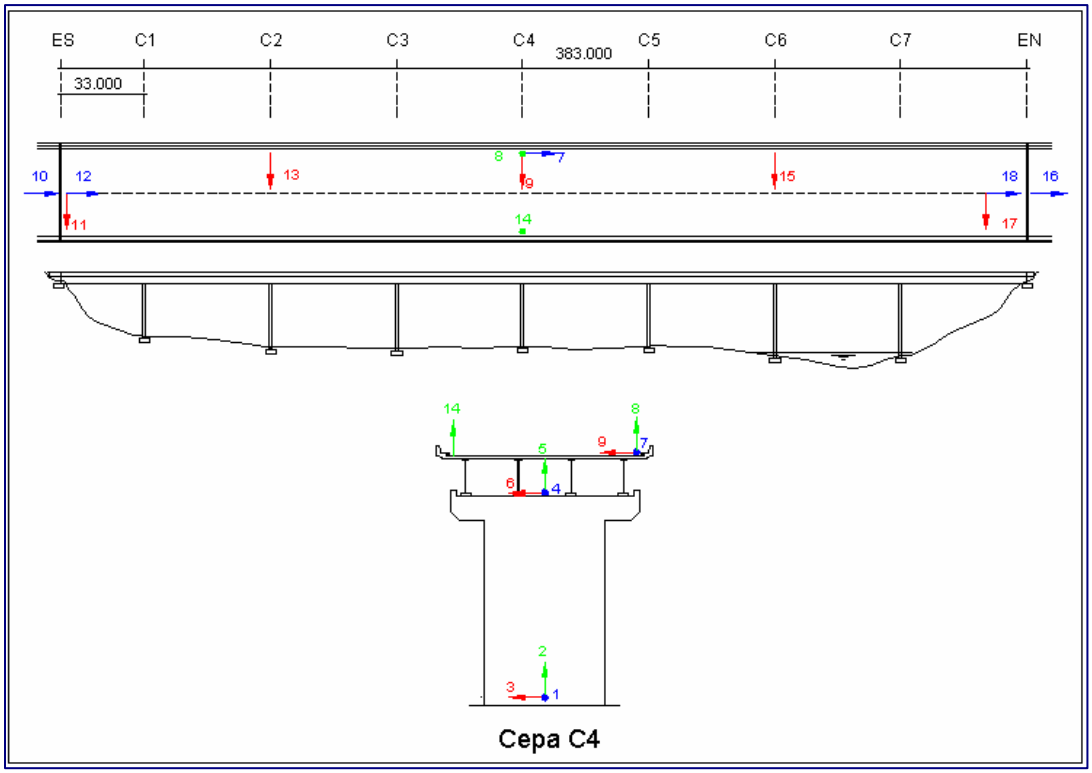

Figure 18. Location of accelerometers

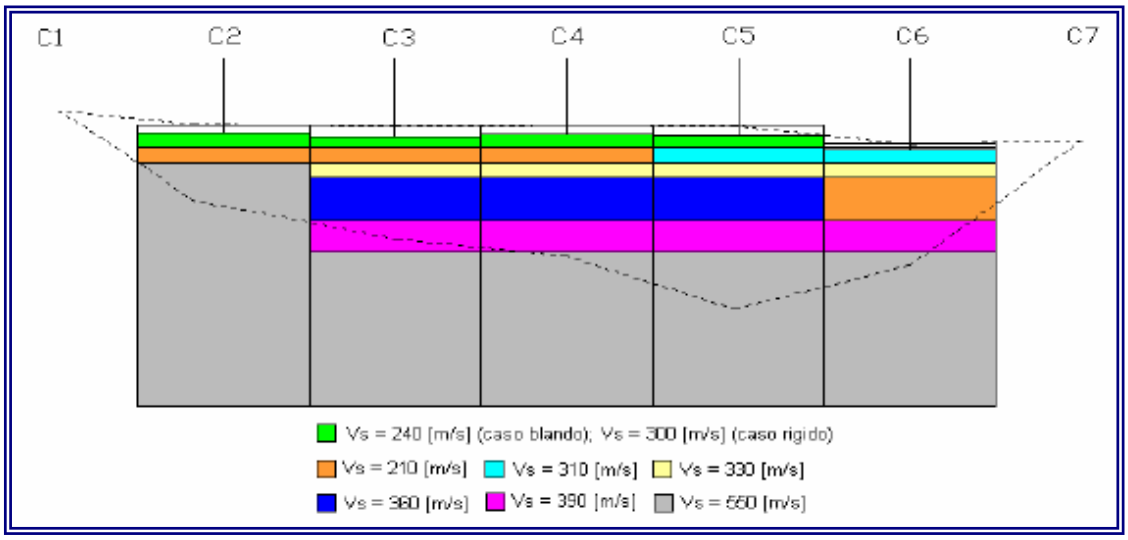

Figure 19. Geotechnical profile of the valley

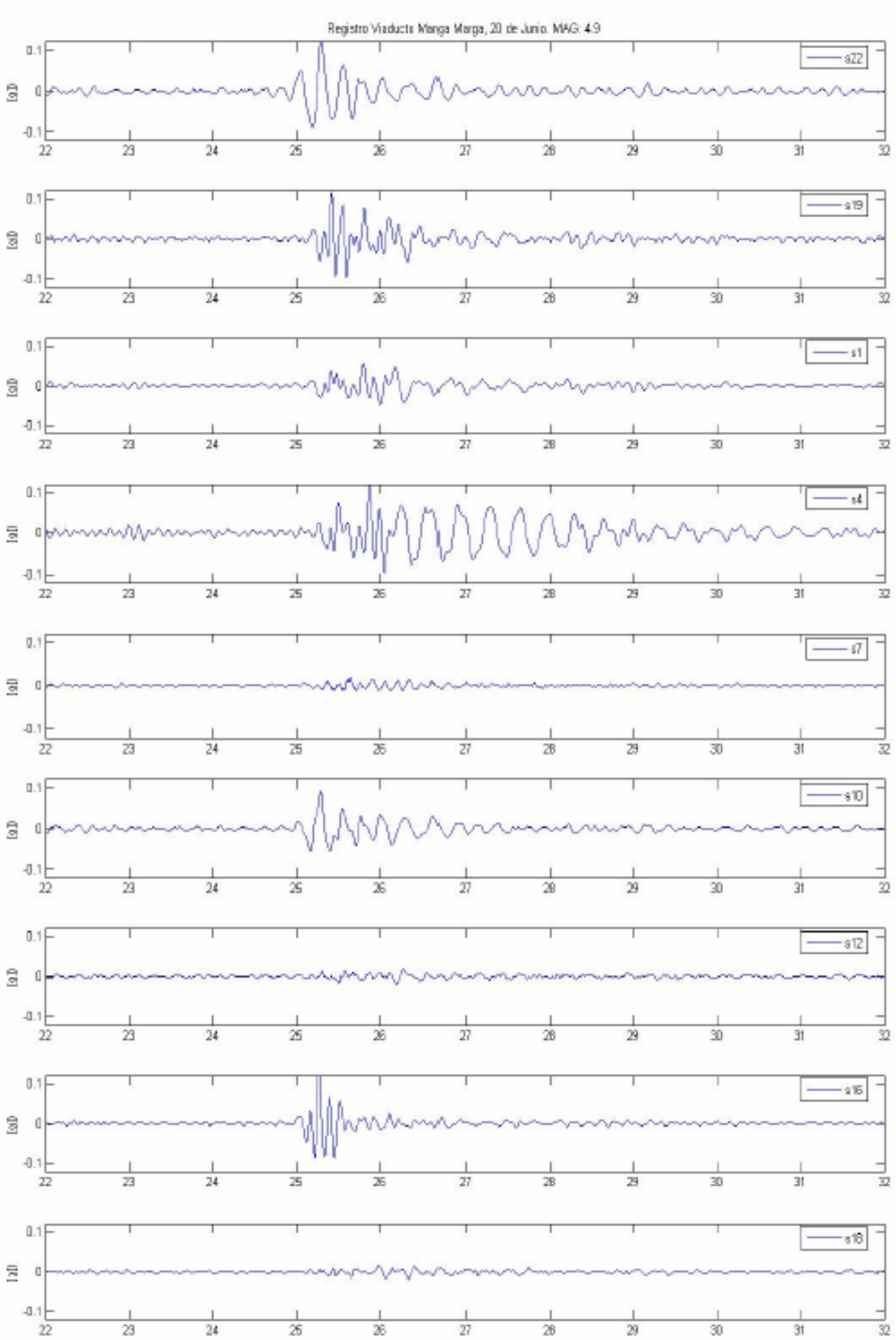

Figure 20. Accelerations registered in longitudinal direction (channels 22, 19, 1, 4, 7, 10, 12, 16, and 18)

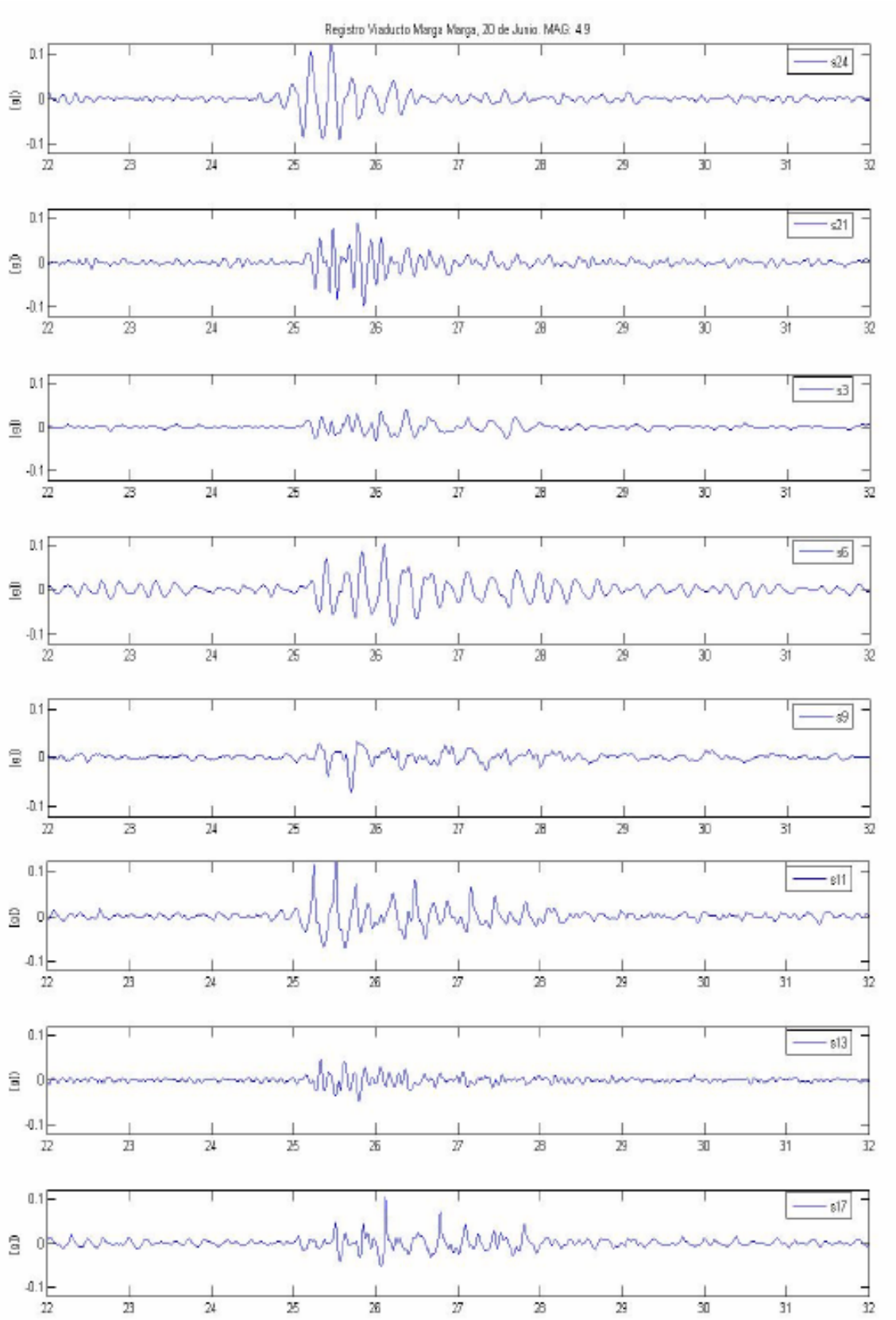

Figure 21. Accelerations registered in transversal direction (channels 24, 21, 3, 6, 9, 11, 13, and 17)

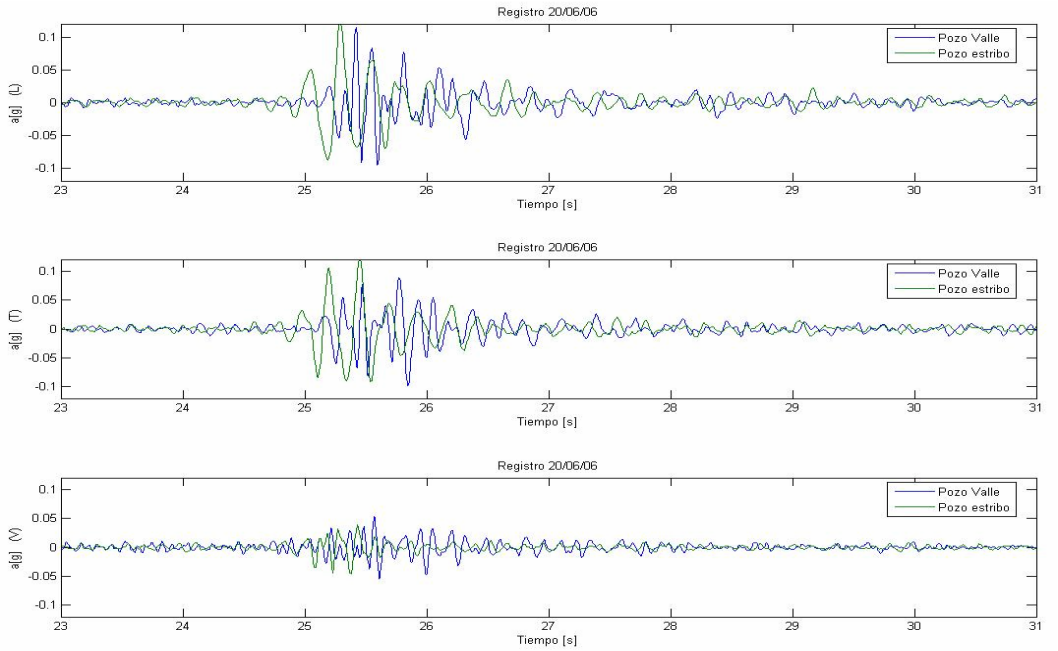

Figure 22. Records on rock (Pozo estribo) and at the valley surface (Pozo valle), near pier C4, for M=4.9 June 20, 2006 earthquake.

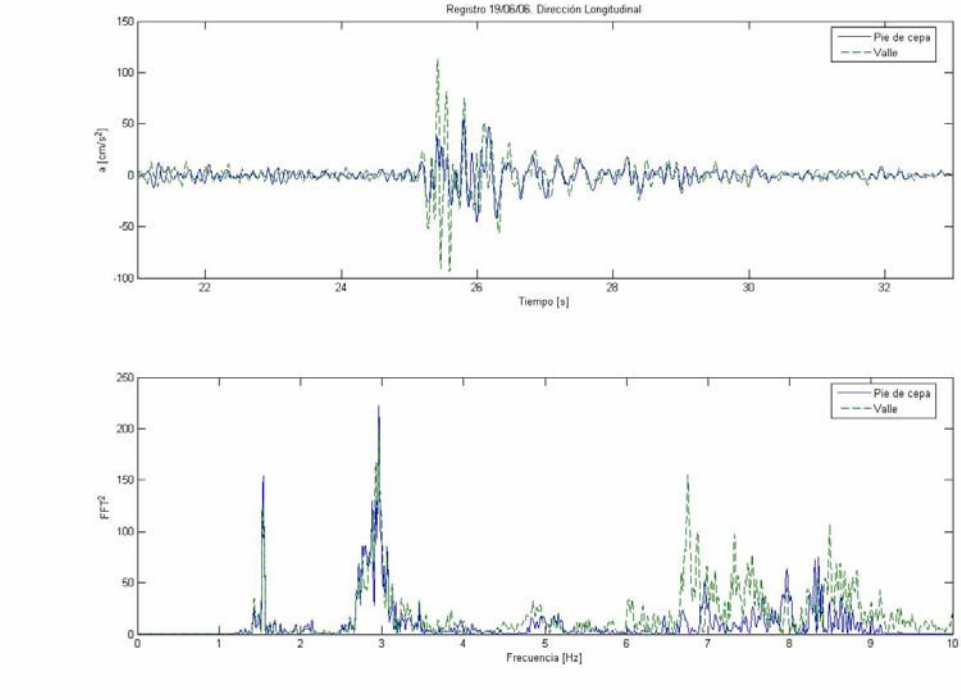

Figure 23. Records at foundation of pier C4 and at free field in the valley. Longitudinal direction.

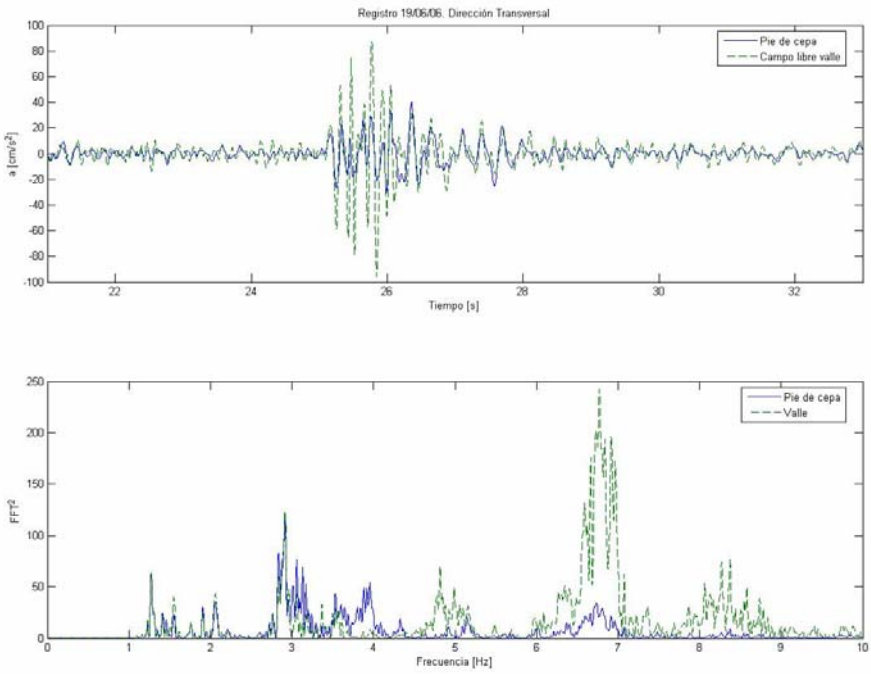

Figure 24. Records at foundation of pier C4 and at free field in the valley. Transverse direction.

Table 9. Comparison of error committed for analytical records from two models: a) considering differential motions between supports and b) with uniform earthquake input.

		REGISTERED	MODEL		UNIFORM EARTHQUAKE INPUT	
Sensor (Acc.)	Dir.	Displac. (cm)	Displac. (cm)	Error (%)	Displac. (cm)	Error (%)
Canal 4	L	0.239	0.171	29	0.169	29
Canal 5	V	0.039	0.034	13	0.035	10
Canal 6	T	0.162	0.145	10	0.128	21
Canal 7	L	0.062	0.040	35	0.035	43
Canal 8	V	0.050	0.050	0	0.048	4
Canal 9	T	0.184	0.171	7	0.245	33
Canal 11	T	0.157	0.118	25	0.229	45
Canal 12	L	0.054	0.031	43	0.032	41
Canal 13	T	0.110	0.148	34	0.207	88
Canal 14	V	0.052	0.051	1	0.054	5
Canal 15	V	0.063	0.064	2	0.055	12
Canal 18	L	0.057	0.043	24	0.043	24
Average				**19**	**30**	

ACKNOWLEDGEMENTS

The authors wish to express their appreciation to the University of Chile for their financial support, to the Ministry of Public Works (Technology Innovation Program) and to Fondecyt research fund (Project Nº 1061265).

REFERENCES

Araya, R. & Saragoni, G. R. (1984) "Earthquake Accelerogram Destructiveness Potencial Factor", 8th. World Conference on Earthquake Engineering, San Francisco, U.S.A.

Biggs, J.M., (1964), *Introduction to Structural Dynamics*, McGraw Hill, New York.

Brull, J. (2005) Shaking table testing of scaled model of shear wall building equipped with rubber bearings, Civil Engineer Thesis, University of Chile. [in Spanish]

Deb, K., A. Pratap, S. Agrawal, and T. Meyarivan, (2002), "A Fast Elitist Non-Dominated Sorting Genetic Algorithm for Multi-Objective Optimization: NSGA-II," *IEEE Transaction on Evolutionary Computation*, **6**(2), 182-197.

Kim, H.-S., and P.N. Roschke, (2006), "Design of Fuzzy Logic Controller for Smart Base Isolation System Using Genetic Algorithm," *Engineering Structures*, **28**(1), 84-96.

MATLAB, The Mathworks, Inc., Natick, Massachusetts (2006).

Muñoz, R, (2005) "Shaking table testing of scaled model of shear wall building equipped with friction bearings". Civil Engineer Thesis, University of Chile. [in Spanish]

Oh, J., P.N. Roschke, P.-Y. Lin, J.D. Carlson, and K. Sunakoda, (2004), "Experimental Behavior and Neuro-Fuzzy Modeling of 30-ton Magnetorheological Damper," *Journal of Civil Engineering*, KSCE, **8**(2), 213-219.

Roschke, P.N., and V. Likhitruangslip, (2003), "Fuzzy Modeling of 30-Ton Magnetorheological Damper Behavior," *Proceedings of the ASCE 2003 Structures Congress*, Seattle, Washington.

Sarrazin, M, M. O. Moroni, P. Soto (2001), « Applications on Seismic Isolation and Energy Dissipation in Bridges in Chile and Venezuela », *7th International Seminar on Seismic Isolation, Passive Energy Dissipation and Active Control of Vibrations of Structures*, Assisi, Italy, October 2 – 5, 2001.

Ungar, E.E., J.A. Zapfe, and J.D. Kemp, (2004), "Predicting Footfall-Induced Vibrations of Floors," *Sound and Vibration*, 16-21.

Valdivieso, J.T. (2006), "Experimental Checking of Seismic Behavior of a Frame Model with Cooper-base SMA Dissipapors". Civil Engineer Thesis, University of Chile [in Spanish].